Contribution from the Chemistry Department,
University of Virginia, Charlottesville, Virginia 22901

Optical Absorption and Circular Dichroism Spectra, Transition Line Strengths, and Crystal-Field Analysis of the Er^{3+} $4f^{11}$ Electronic Energy-Level Structure in Trigonal $Na_3[Er(C_4H_4O_5)_3]\cdot 2NaClO_4\cdot 6H_2O$

Karl A. Schoene, John R. Quagliano, and F. S. Richardson*

Received January 8, 1991

Locations and assignments of 65 crystal-field levels are reported for Er^{3+} in the trigonal $Na_3[Er(ODA)_3]\cdot 2NaClO_4\cdot 6H_2O$ system (ODA = oxydiacetate). These levels were located and assigned from transitions observed in σ- and π-polarized *orthoaxial* absorption spectra and in *axial* absorption and circular dichroism (CD) spectra obtained on single-crystal samples at temperatures between 15 and 298 K. The absorption measurements spanned the 6000–40 000-cm^{-1} spectral region, and the CD measurements spanned the 15 000–25 000-cm^{-1} region. The empirical energy-level data are analyzed in terms of a parametrized model Hamiltonian for the $4f^{11}$ electronic configuration of Er^{3+}, assumed to be perturbed by a crystal field of trigonal-dihedral (D_3) symmetry. Parametric fits of calculated-to-empirical energy-level data yield a root-mean-square deviation of 9.6 cm^{-1} (between calculated and observed energies). The Hamiltonian parameter values obtained from these energy-level analyses are compared with results obtained from similar analyses of Er^{3+} in other crystalline hosts *and* of other lanthanide (Ln^{3+}) ions in the $Na_3[Ln(ODA)_3]\cdot 2NaClO_4\cdot 6H_2O$ system. Polarized absorption line-strength data are reported for 33 transitions that originate from the lowest crystal-field level of the $^4I_{15/2}$ (ground) multiplet of Er^{3+} and terminate on crystal-field levels of eight different *J*-multiplet manifolds located between 15 000 and 27 000 cm^{-1}. Variable-temperature absorption measurements indicate that the *J*-multiplet baricenter energies *and* the crystal-field splittings within *J*-multiplet manifolds are essentially invariant over the 15 to 298 K temperature range. However, at sample temperatures below ~100 K, the polarized absorption and circular dichroism spectra show evidence that crystal structure about the Er^{3+} sites deviates from the room-temperature structure.

Introduction

The isomorphous series of compounds $Na_3[Ln(C_4H_4O_5)_3]\cdot 2NaClO_4\cdot 6H_2O$ formed by trivalent lanthanide ions (Ln^{3+}) and oxydiacetate dianions ($C_4H_4O_5^{2-} \equiv {}^-OOCCH_2OCH_2COO^-$) in aqueous solution with perchloric acid have received considerable attention as model systems for investigating ligand-field effects on lanthanide $4f^N$ electronic state structure and optical properties.[1-46] Optical-quality single crystals of these compounds are readily grown from aqueous solution, and at room temperature the crystals belong to the space group $R32$.[47-50] The Ln^{3+} ions are located at sites with D_3 symmetry, and each Ln^{3+} ion is coordinated to three oxydiacetate (ODA) ligands to form a tris-terdentate $Ln(ODA)_3^{3-}$ complex of trigonal-dihedral (D_3) point-group symmetry. The LnO_9 coordination cluster in these complexes forms a slightly distorted tricapped trigonal-prism polyhedron (of D_3 symmetry), with the top and bottom triangles defined by carboxylate oxygen atoms and the capping positions (on normals to the rectangular faces) occupied by ether oxygen atoms. The backbone of each bicyclic Ln(ODA) chelate ring system is nearly planar and stretches diagonally across a rectangular face of the LnO_9 trigonal-prism structure. The chelate rings contain highly anisotropic electronic charge distributions, and their interactions with the lanthanide 4f electrons produce effects not ordinarily seen in structurally simpler systems. Furthermore, single crystals of $Na_3[Ln(ODA)_3]\cdot 2NaClO_4\cdot 6H_2O$ grow (spontaneously) in two enantiomorphic forms, which differ with respect to the absolute configuration of their constituent $Ln(ODA)_3^{3-}$ complexes *and* the chiral (left-handed or right-handed) arrangement of these complexes about the trigonal axis of the crystal.[50] Therefore, these systems exhibit *chiroptical* properties that may be exploited in characterizing spectroscopic state structure and transition mechanisms.[41]

Optical and chiroptical studies of $Na_3[Ln(ODA)_3]\cdot 2NaClO_4\cdot 6H_2O$ systems have proved to be extraordinarily useful for investigating lanthanide $4f^N$ electronic state structure and 4f–4f optical transition processes in a relatively complex, but structurally well-defined, ligand environment. The most thorough and comprehensive spectroscopic studies have been reported for the neodymium,[35,39,40,51] samarium,[27-30,51] europium,[33,34] gadolinium,[42,45] and holmium[38,43,44] members of the $Na_3[Ln(ODA)_3]\cdot 2NaClO_4\cdot 6H_2O$ series (denoted hereafter by LnODA). In the present paper, we report optical absorption and circular dichroism results obtained for ErODA, and we also report the first detailed crystal-field analysis of the $4f^{11}$ (Er^{3+}) electronic energy-level

* To whom correspondence should be addressed.

(1) Norden, B.; Grenthe, I. *Acta Chem. Scand.* **1972**, *26*, 407.
(2) Sen, A. C.; Bera, S. C.; Chowdhury, M. *Chem. Phys. Lett.* **1977**, *46*, 594.
(3) Banerjee, A. K.; Mukherjee, R. K.; Chowdhury, M. *J. Chem. Soc., Faraday Trans. 2* **1979**, *75*, 337.
(4) Schwartz, R. W.; Banerjee, A. K.; Sen, A. C.; Chowdhury, M. *J. Chem. Soc., Faraday Trans. 2* **1980**, *76*, 620.
(5) Banerjee, A. K.; Sen, A. C.; Chowdhury, M. *Chem. Phys. Lett.* **1980**, *69*, 592.
(6) Kuroda, R.; Mason, S. F.; Rosini, C. *Chem. Phys. Lett.* **1980**, *70*, 11.
(7) Kuroda, R.; Mason, S. F.; Rosini, C. *J. Chem. Soc., Faraday Trans. 2* **1981**, *77*, 2125.
(8) Sen, A. C.; Chowdhury, M.; Schwartz, R. W. *J. Chem. Soc., Faraday Trans. 2* **1981**, *77*, 1293.
(9) Banerjee, A. K.; Schwartz, R. W.; Chowdhury, M. *J. Chem. Soc., Faraday Trans. 2* **1981**, *77*, 1635.
(10) Roy, D. S.; Bhattacharyya, K.; Gupta, A. K.; Chowdhury, M. *Chem. Phys. Lett.* **1981**, *77*, 422.
(11) Schwartz, R. W.; Banerjee, A. K.; Chowdhury, M.; Kuroda, R. *J. Chem. Soc., Faraday Trans. 2* **1981**, *77*, 557.
(12) Sen, A. C.; Chowdhury, M. *Chem. Phys. Lett.* **1981**, *79*, 165.
(13) Richardson, F. S.; Saxe, J. D.; Davis, S. A.; Faulkner, T. R. *Mol. Phys.* **1981**, *42*, 1401.
(14) Morley, J. P.; Saxe, J. D.; Richardson, F. S. *Mol. Phys.* **1982**, *47*, 379.
(15) Saxe, J. D.; Morley, J. P.; Richardson, F. S. *Mol. Phys.* **1982**, *47*, 407.
(16) Chatterjee, P. K.; Chowdhury, M. *J. Chem. Soc., Faraday Trans. 2* **1982**, *78*, 429.
(17) Richardson, F. S.; Faulkner, T. R. *J. Chem. Phys.* **1982**, *76*, 1595.
(18) Saxe, J. D.; Faulkner, T. R.; Richardson, F. S. *J. Chem. Phys.* **1982**, *76*, 1607.
(19) Banerjee, A. K.; Schwartz, R. W. *J. Chem. Soc., Faraday Trans. 2* **1983**, *79*, 755.
(20) Kirby, A. F.; Richardson, F. S. *J. Phys. Chem.* **1983**, *87*, 2557.
(21) Karmakar, B.; Roy, D. S.; Bhattacharyya, K.; Samanta, A.; Chowdhury, M. *Chem. Phys. Lett.* **1983**, *97*, 545.
(22) Dallara, J. J.; Reid, M. F.; Richardson, F. S. *J. Phys. Chem.* **1984**, *88*, 3587.
(23) Karmakar, B.; Chatterjee, P. K.; Roy, D. S.; Nath, D.; Chowdhury, M.; Walklyn, B. *Chem. Phys. Lett.* **1984**, *107*, 203.
(24) Albin, M.; Whittle, R. R.; Horrocks, W. DeW, Jr. *Inorg. Chem.* **1985**, *24*, 4591.
(25) Richardson, F. S.; Berry, M. T.; Reid, M. F. *Mol. Phys.* **1986**, *58*, 929.
(26) Berry, M. T.; Richardson, F. S. *J. Less-Common Met.* **1986**, *126*, 251.
(27) Carter, R. C.; Miller, C. E.; Palmer, R. A.; May, P. S.; Metcalf, D. H.; Richardson, F. S. *Chem. Phys. Lett.* **1986**, *131*, 37.
(28) May, P. S.; Reid, M. F.; Richardson, F. S. *Mol. Phys.* **1987**, *61*, 1455.
(29) May, P. S.; Reid, M. F.; Richardson, F. S. *Mol. Phys.* **1987**, *61*, 1471.
(30) May, P. S.; Reid, M. F.; Richardson, F. S. *Mol. Phys.* **1987**, *62*, 341.

0020-1669/91/1330-3803$02.50/0

structure in this system. The optical absorption results were obtained from both unpolarized *axial* and σ- and π-polarized *orthoaxial* absorption intensity measurements carried out over the 6000–40 000-cm^{-1} spectral range, and the circular dichroism results were obtained from *axial* circular dichroic intensity measurements performed over the 15 000–25 000-cm^{-1} spectral region. Absorption line strengths are reported for 33 transitions that originate from the lowest crystal-field level of the $^4I_{15/2}$ (ground) multiplet of Er^{3+} and terminate on crystal-field levels of eight different J-multiplet manifolds located between 15 000 and 27 000 cm^{-1}.

Among the 108 crystal-field energy levels split out of the 24 lowest-energy J-multiplets of the Er^{3+} $4f^{11}$ electronic configuration, 65 are located and assigned from the optical absorption and circular dichroism spectra. The assigned levels are analyzed in terms of a parametrized model Hamiltonian that assumes trigonal-dihedral (D_3) site symmetry for Er^{3+} in $Na_3[Er(ODA)_3]\cdot 2NaClO_4\cdot 6H_2O$. Parametric fits of calculated-to-empirical energy-level data yield a root-mean-square deviation of 9.6 cm^{-1} (between the calculated and experimentally determined energies of assigned crystal-field levels), and they give values for the atomic and crystal-field Hamiltonian parameters that are compatible with results reported for Er^{3+} in other crystalline hosts *and* for other Ln^{3+} ions in $Na_3[Ln(ODA)_3]\cdot 2NaClO_4\cdot 6H_2O$ (vide infra).

The measurements reported in this paper were carried out on crystals at temperatures between approximately 15 and 298 K. Five of the eight crystal-field levels split out of the $^4I_{15/2}$ (ground) multiplet of the Er^{3+} $4f^{11}$ electronic configuration were located and assigned from the variable-temperature absorption spectra. These five levels are located at 0 (ground), 42, 148, 178, and 208 cm^{-1}, and they are assigned to crystal-field states of E″, E′, E′, E″, and E′ symmetry, respectively (where E′ and E″ denote irreducible representations in the D_3 double-group). Calculations indicate that the remaining three crystal-field levels of the $^4I_{15/2}$ multiplet manifold are located above 330 cm^{-1}, and no transitions from these levels were observed in our absorption spectra. Locations and assignments of crystal-field levels split out of *excited* J-multiplets were based almost entirely on absorption spectra measured at sample temperatures below 50 K. The transitions observed in these spectra originate from either the ground (E″) or first excited (E′) crystal-field level of the $^4I_{15/2}$ (ground) multiplet manifold. Absorption line strengths were determined only for transitions that originate from the ground crystal-field level.

The ErODA crystals retain macroscopic uniaxial symmetry over the entire 298–15 K temperature range represented in our absorption measurements, and this conforms with the macroscopic symmetry properties observed for other LnODA systems. However, there is evidence that at least several of these systems undergo low-temperature structural phase transitions in which the crystal space group changes from $R32$ to $P321$, and the lanthanide site symmetry is reduced from D_3 to C_2 (attributable to movement of the Na^+ ions off 3-fold axes).[11,14,35,46] This type of structural change is relatively easy to detect in the 4f–4f optical spectra of LnODA systems with an *even* number of 4f electrons, because in these systems the crystal-field levels that are doubly degenerate in D_3 symmetry generally split into resolvable nondegenerate components when the lanthanide site symmetry is reduced to C_2.[14,43] However, for systems with an *odd* number of 4f electrons, all crystal-field levels are Kramers doublets and their degeneracy is not removed by a lowering of the lanthanide site symmetry. The variable-temperature absorption spectra measured for ErODA crystals indicate that the J-multiplet baricenter energies *and* the crystal-field splittings within J-multiplet manifolds are essentially invariant to temperature. Furthermore, the relative line strengths of transitions between crystal-field levels do not show a significant temperature dependence. However, comparisons of the σ- versus π-polarized absorption spectra obtained at temperatures below 100 K reveal significant polarization scrambling in the transitions. These observations are compatible with a structural model in which the "effective" ligand-field potential sensed by the 4f electrons reflects the D_3 point-group symmetry of the $Er(ODA)_3^{3-}$ complexes but in which the trigonal axes of the $Er(ODA)_3^{3-}$ complexes (three per unit cell) are tilted away from the crystallographic 3-fold symmetry axis. We will defer further comment on this model until later in the paper. Suffice it to state here that the crystal-field energy-level structure of Er^{3+} in $Na_3[Er(ODA)_3]\cdot 2NaClO_4\cdot 6H_2O$ can be satisfactorily modeled by a Hamiltonian that reflects effective D_3 ligand-field symmetry.

Experimental Section

Single crystals of $Na_3[Er(ODA)_3]\cdot 2NaClO_4\cdot 6H_2O$ were grown from aqueous solution following the methods of Albertsson.[47,48] Damp Whatman glass-microfiber filter paper was used to polish crystals to a thickness and shape suitable for optical measurements. Variable-temperature measurements between 15 and 298 K were carried out with the crystal sample mounted at the cold station in the sample compartment of a CTI-Cryogenics closed-cycle helium refrigerator and cryostat. The crystal was mounted on a one-piece copper mount by using Crycon grease (Air Products, Inc.) and indium foil, and the copper mount was attached to the cold head of the refrigerator, with strips of indium providing a thermally conductive interface. Cold-head temperature was controlled by using a Lake Shores temperature controller (Model DRC-70).

Absorption spectra were recorded with either a Cary Model 17D or a Cary Model 2415 UV–vis–near-IR spectrophotometer. Unpolarized *axial* spectra were measured over the 250–1700-nm wavelength range, and σ- and π-polarized *orthoaxial* spectra were measured over the 370–1700-nm wavelength range. The spectral resolution achieved in these measurements was ≤0.1 nm, and sample thicknesses (optical path lengths) were chosen such that the largest recorded absorbances, in any given spectral region of interest, were less than 70% of the spectrophotometer's full-scale absorbance limit. Optical transmission spectra in the 250–370-nm wavelength region were also measured with a lab-built, high-resolution spectrophotometer normally used for emission and Raman spectroscopic measurements. In these experiments, broad-band radiation from a xenon arc lamp was passed through the crystal sample, and the transmitted radiation was then dispersed with a 0.75-m Spex double-grating monochromator in which the gratings are blazed for first-order diffraction at 500 nm. The *second-order* output of the monochromator was scanned to obtain an optical transmission spectrum, and this spectrum was then converted to an absorbance spectrum by correcting for the arc-lamp output profile and the second-order dispersion characteristics of the monochromator. The spectral resolution achievable in these transmission measurements is at least 1 order of magnitude better than that obtainable with the Cary 17D and 2415 spectrophotometers, but quantitative intensity data are more easily (and accurately) determined from the Cary spectra.

Circular dichroism spectra were measured with a custom-built, double-beam CD/absorption spectrophotometer constructed in Professor P.

(31) Vala, M.; Nath, D.; Chowdhury, M.; Wierzbicki, A.; Sen, A. C. *Chem. Phys. Lett.* **1987**, *134*, 610.
(32) Karmakar, B.; Chatterjee, P. K.; Basu, S.; Chowdhury, M. *Bull. Chem. Soc. Jpn.* **1987**, *60*, 2993.
(33) Berry, M. T.; Schwieters, C.; Richardson, F. S. *Chem. Phys.* **1988**, *122*, 105.
(34) Berry, M. T.; Schwieters, C.; Richardson, F. S. *Chem. Phys.* **1988**, *122*, 125.
(35) Vala, M.; Szczepanski, J.; Banerjee, A. K.; Chowdhury, M. *Chem. Phys.* **1989**, *134*, 149.
(36) Schoene, K. A.; Richardson, F. S. *J. Less-Common Met.* **1989**, *148*, 305.
(37) Metcalf, D. H.; Richardson, F. S. *J. Less-Common Met.* **1989**, *148*, 321.
(38) Moran, D. M.; DePiante, A.; Richardson, F. S. *J. Less-Common Met.* **1989**, *148*, 297.
(39) May, P. S.; Jayasankar, C. K.; Richardson, F. S. *Chem. Phys.* **1989**, *138*, 123.
(40) May, P. S.; Jayasankar, C. K.; Richardson, F. S. *Chem. Phys.* **1989**, *138*, 139.
(41) Richardson, F. S. *J. Less-Common Met.* **1989**, *149*, 161.
(42) Kundu, T.; Banerjee, A. K.; Chowdhury, M. *Phys. Rev. B* **1990**, *41*, 10911.
(43) Moran, D. M.; De Piante, A.; Richardson, F. S. *Phys. Rev. B* **1990**, *42*, 3317.
(44) Moran, D. M.; Richardson, F. S. *Phys. Rev. B* **1990**, *42*, 3331.
(45) Stephens, E. M.; Metcalf, D. H.; Berry, M. T.; Richardson, F. S. *Phys. Rev. B*, in press.
(46) Desgupta, S.; Saha, M.; Ghosh, G. *J. Phys. C: Solid State Phys.* **1986**, *19*, 1771.
(47) Albertsson, J. *Acta Chem. Scand.* **1968**, *22*, 1563.
(48) Albertsson, J. *Acta Chem. Scand.* **1970**, *24*, 3527.
(49) Albertsson, J.; Elding, I. *Acta Chem. Scand., Ser. A* **1977**, *31*, 21.
(50) Fronczek, F. R.; Banerjee, A. K.; Watkins, S. F.; Schwartz, R. W. *Inorg. Chem.* **1981**, *20*, 2745.
(51) May, P. S. Ph.D. Dissertation, University of Virginia, 1988.

Table I. Electric (μ) and Magnetic (m) Dipole Selection Rules

transition	axial spectra	orthoaxial spectra: σ-polarized	orthoaxial spectra: π-polarized
$E' \rightarrow E'$	(μ_x,μ_y); (m_x,m_y)	(μ_x,μ_y); m_z	μ_z; (m_x,m_y)
$E'' \rightarrow E''$	forbidden	m_z	μ_z
$E' \leftrightarrow E''$	(μ_x,μ_y); (m_x,m_y)	(μ_x,μ_y)	(m_x,m_y)

N. Schatz's laboratory at the University of Virginia. These measurements were carried out over the 400–670-nm wavelength range, on crystals aligned with their unique, crystallographic c axis parallel to the direction of light propagation (i.e., the *axial* optical configuration).

Optical Selection Rules and Line Assignments

All energy levels split out of the $4f^{11}$ electronic configuration of Er^{3+} in a trigonal-dihedral (D_3) crystal field are doubly degenerate (Kramers doublets), and each may be classified as having either E′ and E″ symmetry in the D_3 double-group (D_3^*), where E′ and E″ denote irreducible representation (irrep) labels in this group. Therefore, all transitions between crystal-field levels may be classified (by symmetry) as $E' \rightarrow E'$, $E'' \rightarrow E''$, or $E' \leftrightarrow E''$. The direct products of the E′ and E″ irreps, with themselves and with each other, are $E' \times E' = [A_1] + A_2 + E$, $E'' \times E'' = [A_1] + A_1 + 2A_2$, and $E' \times E'' = 2E$. With choice of a Cartesian coordinate system in which the z axis is coincident with the C_3 symmetry axis of our trigonal (D_3) system, the x and y components of both the electric and magnetic dipole moment operators (denoted here by μ and $\mathbf{m}$, respectively) transform as E, whereas the z component of each transforms as A_2. Given these symmetry properties, electric and magnetic dipole selection rules are easily deduced for the $E' \rightarrow E'$, $E'' \rightarrow E''$, and $E' \leftrightarrow E''$ transition types in axial (α) and orthoaxial (σ- and π-polarized) optical absorption spectra of $Na_3[Er(ODA)_3]\cdot 2NaClO_4\cdot 6H_2O$. Under conditions in which the Er^{3+} site symmetry is D_3 (with the trigonal axis aligned parallel to the crystallographic c axis), these selection rules are as shown in Table I.

Among the 23 multiplet-to-multiplet transition manifolds surveyed in our absorption measurements, all but three are expected to exhibit intensities that are overwhelmingly dominated by electric dipole contributions. The three exceptions are $^4I_{15/2} \rightarrow {}^4I_{13/2}$ (centered near 6700 cm^{-1}), $^4I_{15/2} \rightarrow {}^2K_{15/2}$ (near 27 850 cm^{-1}), and $^4I_{15/2} \rightarrow {}^2K_{13/2}$ (near 33 100 cm^{-1}), each of which might be expected to exhibit comparable electric *and* magnetic dipole intensities.[52] For the predominantly electric dipole transitions (between crystal-field levels), symmetry assignments can be made straightforwardly by comparing the relative intensities of lines observed in the unpolarized axial spectra and the σ- versus π-polarized orthoaxial spectra. According to the selection rules of Table I, $E'' \rightarrow E''$ electric dipole transitions will appear only in the π-polarized spectra, $E' \rightarrow E''$ electric dipole transitions will appear only in the axial and the σ-polarized spectra, and $E' \rightarrow E'$ electric dipole transitions may appear in all three types of spectra. It was noted earlier (in the Introduction) that a partial breakdown of these selection rules is observed in the low-temperature absorption spectra recorded for $Na_3[Er(ODA)_3]\cdot 2NaClO_4\cdot 6H_2O$. Some polarization "scrambling" or "leakage" is observed in many transition regions of the σ- and π-polarized orthoaxial spectra. However, in all cases the degree of polarization observed for any particular transition is sufficiently strong to permit an unambiguous symmetry assignment.

Calculations and Data Analysis

Energy Levels. The $4f^{11}$ electronic energy-level structure of Er^{3+} in ErODA was analyzed in terms of a model Hamiltonian that may be written as

$$\hat{H} = \hat{H}_a + \hat{H}_{cf}^+ \quad (1)$$

where $\hat{H}_a$ is defined to incorporate the isotropic parts of $\hat{H}$ (including the spherically symmetric part of the 4f-electron/crystal-field interactions), and $\hat{H}_{cf}^+$ is defined to represent the nonspherically symmetric components of the *even-parity* crystal field.

(52) Schoene, K. A. Ph.D. Dissertation, University of Virginia, 1989.

We refer to $\hat{H}_a$ as the *atomic* Hamiltonian and call $\hat{H}_{cf}^+$ the *crystal-field* Hamiltonian.

In our model, the $\hat{H}_a$ operator is defined by

$$\hat{H}_a = E_{av} + \sum_k F^k \hat{f}_k + \alpha\hat{L}(\hat{L}+1) + \beta\hat{G}(G_2) + \gamma\hat{G}(R_7) + \sum_i T^i \hat{t}_i + \zeta_{so}\hat{A}_{so} + \sum_k P^k \hat{p}_k + \sum_j M^j \hat{m}_j \quad (2)$$

where $k = 2, 4, 6$, $i = 2, 3, 4, 6, 7, 8$, $j = 0, 2, 4$, and the operators ($\hat{o}$) and their associated parameters are written according to conventional notation *and* meaning (with respect to the interactions they represent).[53,54] We define the crystal-field Hamiltonian as

$$\hat{H}_{cf}^+ = \sum_{k,m}\sum_i B_{km}\hat{u}_{km}(i) \quad (3)$$

where i labels the 4f electrons, $\hat{u}_{km}(i)$ is a one-electron unit-tensor operator, and B_{km} denotes a standard (one-electron) crystal-field interaction parameter. In D_3 symmetry, $\hat{H}_{cf}^+$ may be defined in terms of just six B_{km} parameters: $(k,m) = (2,0), (4,0), (4,3), (6,0), (6,3)$, and $(6,6)$.

The atomic Hamiltonian, defined by the expression (2), contains 20 parameters (including E_{av}), and the crystal-field Hamiltonian, defined by the expression (3) and assuming D_3 symmetry, contains six parameters. The *complete* $\hat{H}_a$ operator was used in all of our energy level calculations, although not all of the 20 parameters contained in this operator were treated as free variables in performing parametric fits of calculated-to-experimental energy level data (vide infra). In all of our energy-level calculations, the total (atomic + crystal-field) Hamiltonian was diagonalized within the *complete* $f^{11}SLJM_J$ basis set (comprised of 364 states).

Absorption Intensities. Intensities of transitions between crystal-field levels are reported here in terms of transition line strengths. Separate line strengths were determined for transitions observed in unpolarized *axial* (α) absorption spectra and in σ- and π-polarized *orthoaxial* absorption spectra. For a transition between levels A (initial) and B (final), the respective line strengths were determined according to the following expressions:

$$S_{AB}(\alpha) = 3.063 \times 10^{-39}[g_A/X_A(T)]\int_{A\rightarrow B}\epsilon_\alpha(\bar{\nu},T)\,d\bar{\nu}/\bar{\nu} \text{ (esu}^2\text{ cm}^2\text{)} \quad (4)$$

$$S_{AB}(p) = 3.063 \times 10^{-39}[g_A/X_A(T)]\int_{A\rightarrow B}\epsilon_p(\bar{\nu},T)\,d\bar{\nu}/\bar{\nu} \text{ (esu}^2\text{ cm}^2\text{)} \quad (5)$$

Here p denotes σ or π polarization, g_A is the electronic degeneracy of level A, $X_A(T)$ is the fractional thermal (Boltzmann) population of level A at temperature T, ϵ_α and ϵ_p (p = σ or π) are molar decadic absorption coefficients measured in the axial and orthoaxial absorption experiments, respectively, the integrations are over the $A \rightarrow B$ transition line width, and $\bar{\nu}$ denotes the wavenumber (cm^{-1}) of the radiation. The molar decadic absorption coefficient (ϵ) is related to sample transmittance (T) and decadic absorbance (A) according to $\log_{10}(1/T) = A = \epsilon c_m l$, where c_m denotes the molar concentration of absorbing species (M ≡ mol/L), l denotes sample thickness (in cm), and ϵ has the units $M^{-1}\ cm^{-1}$ (*or* equivalently cm^2/mmol). The Er^{3+} concentration in $Na_3[Er(ODA)_3]\cdot 2NaClO_4\cdot 6H_2O$ is 2.176 mol/L.

If we assume that only electric dipole and magnetic dipole transition processes contribute to the observed line intensities, then the line strengths (S_{AB}) may be expressed as follows:

$$S_{AB}(\alpha) = \chi_\alpha D^e_{AB,1} + \chi_\alpha' D^m_{AB,1} \quad (6)$$

$$S_{AB}(\sigma) = \chi_\sigma D^e_{AB,1} + \chi_\sigma' D^m_{AB,0} \quad (7)$$

$$S_{AB}(\pi) = \chi_\pi D^e_{AB,0} + \chi_\pi' D^m_{AB,1} \quad (8)$$

Here χ and χ' are correction factors for bulk (sample) refractivity

(53) Crosswhite, H. M.; Crosswhite, H. *J. Opt. Soc. Am. B* **1984**, *1*, 246.
(54) Carnall, W. T.; Goodman, G. L.; Rajnak, K.; Rana, R. S. *J. Chem. Phys.* **1989**, *90*, 3443.

effects on the electric dipole and magnetic dipole components of the radiation field, and

$$D^{e}_{AB,q} = |\sum_{a}\sum_{b}\langle Aa|\mu_q|Bb\rangle|^2 \quad (9)$$

$$D^{m}_{AB,q} = |\sum_{a}\sum_{b}\langle Aa|m_q|Bb\rangle|^2 \quad (10)$$

where the summations are over the degenerate components of levels A and B, μ_q and m_q denote components of the electric and magnetic dipole moment operators expressed in a spherical basis ($q = 0, \pm 1$), and the $q = 0$ basis vector is defined to be parallel to the 3-fold symmetry axis (the unique axis) of the crystal.

All of the line strengths reported in this paper are for transitions that originate from the ground crystal-field level of the $^4I_{15/2}$ multiplet, and all were determined from absorption intensity measurements performed on samples at 20 ± 2 K.

Circular Dichroic Intensities. Circular dichroism (CD) is defined as the differential absorption of left- and right-circularly polarized light, and experimentally measured CD intensities are normally expressed in terms of $\Delta\epsilon = \epsilon_L - \epsilon_R$ (the difference in molar decadic absorption coefficients for left- and right-circularly polarized light). Contributions to CD intensity from individual optical transitions are frequently expressed in terms of transition rotatory strengths. Within the context of the present study, transition rotatory strengths are defined according to

$$R_{AB}(\alpha) = 2.297 \times 10^{-39}[g_A/X_A(T)\bar{\chi}_\alpha]\int_{A\rightarrow B}\Delta\epsilon_\alpha(\bar{\nu},T)\,d\bar{\nu}/\bar{\nu}\ (\text{esu}^2\ \text{cm}^2) \quad (11)$$

where the integration is over the CD band (plotted as $\Delta\epsilon_\alpha$ versus $\bar{\nu}$) assigned to the transition $A \rightarrow B$, g_A is the degeneracy of the initial level A, $X_A(T)$ is the fractional thermal population of level A at temperature T, and $\bar{\chi}_\alpha$ denotes a bulk sample refractivity factor (with implicit dependence on $\bar{\nu}$ and T). The α label in eq 11 specifies CD measurements along the optic axis of our uniaxial crystal sample.

The CD and absorption lines associated with a single, purely electronic transition have identical line shapes and line widths. Therefore, expressions (4) and (11) may be combined to obtain

$$g_{cd} = \frac{4\bar{\chi}_\alpha R_{AB}(\alpha)}{3S_{AB}(\alpha)} = \frac{\Delta\epsilon_\alpha(\bar{\nu},T)}{\epsilon_\alpha(\bar{\nu},T)} \quad (12)$$

where g_{cd} defines the absorption (or circular dichroic) *dissymmetry factor* of the transition $A \rightarrow B$ and the $\Delta\epsilon_\alpha/\epsilon_\alpha$ ratio has a constant value within the CD and absorption bands of this transition. To a very good approximation, one may assume that circular dichroism in the 4f–4f transitions of ErODA derives entirely from interferences between electric and magnetic dipole transition amplitudes.[17,41] In this approximation, the transition rotatory strengths can be expressed in terms of electric and magnetic dipole transition moments according to

$$R_{AB}(\alpha) = (3/2)Im\sum_{a}\sum_{b}\sum_{q}q^2\langle Aa|\mu_q|Bb\rangle\langle Aa|m_q|Bb\rangle^* \quad (13)$$

where *Im* signifies the imaginary part of the quantity that follows and all other notation conforms to that defined previously for eqs 9 and 10. Also, in this approximation, the $\bar{\chi}_\alpha$ factor is related to the χ_α and χ_α' factors of eq 6 by $\bar{\chi}_\alpha = (\chi_\alpha\chi_\alpha')^{1/2}$, and these factors may be expressed in terms of refractive index (n_α) according to

$$\chi_\alpha = (n_\alpha^2 + 2)^2/9n_\alpha \qquad \chi_\alpha' = n_\alpha \qquad \bar{\chi}_\alpha = (n_\alpha^2 + 2)/3$$

The spectral regions examined in our circular dichroism experiments do not include any transitions with strong magnetic dipole character, and the CD transition intensities are predicted (and observed) to be relatively weak. Consequently, it was not possible to obtain quantitatively reliable rotatory strength data by direct evaluation of eq 11. However, reasonably accurate absorption dissymmetry factors (g_{cd}) could be determined for many transitions that were fully resolved in the low-temperature ($T <$ 50 K) CD spectra.

Results

Energy Levels. The energy levels located and assigned from our optical absorption and circular dichroism measurements are listed in Table II. The levels are identified with respect to the principal $SLJM_J$ components of their eigenvectors, calculated according to the procedures described earlier (see Calculations and Data Analysis). The "observed" energies listed in Table II were determined from the locations of transitions assigned in our absorption and CD spectra, and they include the appropriate $1/\lambda$(air) to $1/\lambda$(vacuum) wavenumber corrections. The "calculated" energies are eigenvalues of the parametrized Hamiltonian defined by eqs 1–3, with the parameter values shown in Table III. Among the 26 parameters in the Hamiltonian, 22 were treated as variables in performing calculated-to-empirical energy-level fits and 4 were constrained to fixed ratios with one of the freely varying parameters (see the M^2, M^4, P^4, and P^6 parameters in Table III). The root-mean-square deviation between the calculated and observed energies shown in Table II is 9.6 cm^{-1}.

Table IV shows a major-component analysis of the $4f^{11}[SL]J$ (multiplet) state vectors calculated with the atomic Hamiltonian parameters of Table III, and it also lists calculated and observed J-multiplet baricenter energies up to 40 000 cm^{-1}. The root-mean-square deviation between calculated and observed baricenter energies is 5.0 cm^{-1}. Table V shows a comparison of atomic Hamiltonian parameters reported for Er^{3+} in several crystalline hosts, and in Table VI the ErODA crystal-field parameters are compared to those reported for two other systems in which Er^{3+} ions occupy trigonally symmetric sites. Crystal-field parameters determined for six different LnODA systems are compared in Table VII. All of the crystal-field parameter values listed in Tables VI and VII were derived from parametric analyses of empirical energy-level data, and in each case the parameters are defined according to eq 3 (with unit-tensor normalization properties).

Transition Intensities. Polarized line strengths are shown in Table VIII for 33 transitions that originate from the ground crystal-field level of $^4I_{15/2}$ and terminate on crystal-field levels split out of the J-multiplets located between 15 000 and 27 000 cm^{-1}. These line strengths were determined from σ- and π-polarized absorption intensity measurements obtained on crystal samples at 20 K. In our energy-level assignment scheme based on D_3 crystal-field symmetry, the ground crystal-field level of the $^4I_{15/2}$ multiplet manifold has E″ symmetry (see Table II), and each of the transitions listed in Table VIII can be classified as either E″ → E″ or E″ → E′. All of these transitions are expected to occur via a predominantly electric dipole mechanism in which the E″ → E″ transitions are polarized along the trigonal symmetry axis (at each Er^{3+} site) and the E″ → E′ transitions are polarized perpendicular to this axis. If the trigonal axes of all Er^{3+} sites are aligned exactly parallel to the unique crystallographic axis (i.e., the *optic* axis of the crystal), the E″ → E″ transitions should be observed only in π-polarized orthoaxial spectra, whereas the E″ → E′ transitions should be observed only in σ-polarized orthoaxial spectra *and* in axial spectra (see selection rules in Table I).

Each of the E″ → E′ transitions listed in Table VIII is predominantly σ-polarized, and each of the E″ → E″ transitions is predominantly π-polarized in the orthoaxial polarized absorption spectra. However, all of the transitions exhibit some degree of *mixed* ($\sigma + \pi$) polarization, which is reflected in the P (degree of polarization) values given in the last column of Table VIII. Among the 21 E″ → E′ transitions, the average value of $S(\sigma)/S(\pi)$ is 3.35 and the average value of $S(\sigma)/[S(\sigma) + S(\pi)]$ is 0.77, which corresponds to 77% σ-polarized character. Among the 12 E″ → E″ transitions, the average value of $S(\pi)/S(\sigma)$ is 5.67 and the

(55) Couture, L.; Rajnak, K. *Chem. Phys.* **1984**, *85*, 315.
(56) Jayasankar, C. K.; Reid, M. F.; Richardson, F. S. *J. Less-Common Met.* **1989**, *148*, 289.
(57) Jayasankar, C. K.; Reid, M. F.; Richardson, F. S. *Phys. Status Solidi B* **1989**, *155*, 559.
(58) Hammond, R. M. Ph.D. Dissertation, University of Virginia, 1988.

Table II. Calculated and Observed Energy Levels of Er^{3+} in $Na_3[Er(ODA)_3]\cdot 2NaClO_4\cdot 6H_2O$

level no.	term[a]	$2J^a$	$\lvert 2M_J\rvert^a$	Γ^b	energy/cm^{-1} calcd[c]	obsd[d]	Δ^e	level no.	term[a]	$2J^a$	$\lvert 2M_J\rvert^a$	Γ^b	energy/cm^{-1} calcd[c]	obsd[d]	Δ^e
1	^{4}I	15	15	E″	1	0	1	69	^{2}K	15	13	E′	27 861		
2	^{4}I	15	7	E′	42	42	0	70	^{2}K	15	7	E′	27 966		
3	^{4}I	15	1	E′	146	148	−2	71	^{2}K	15	11	E′	27 992		
4	^{4}I	15	3	E″	170	178	−8	72	^{2}K	15	9	E″	27 996		
5	^{4}I	15	5	E′	214	208	6	73	^{2}G	7	1	E′	28 056		
6	^{4}I	15	11	E′	334			74	^{2}G	7	3	E″	28 109		
7	^{4}I	15	9	E″	375			75	^{2}G	7	7	E′	28 112		
8	^{4}I	15	13	E′	441			76	^{2}G	7	5	E′	28 114		
9	^{4}I	13	13	E′	6 598	6 593	5	77	^{2}P	3	3	E″	31 593	31 594	−1
10	^{4}I	13	5	E′	6 644	6 642	2	78	^{2}P	3	1	E′	31 604	31 614	−10
11	^{4}I	13	3	E″	6 659	6 650	9	79	^{2}K	13	1	E′	32 970		
12	^{4}I	13	1	E′	6 682	6 670	12	80	^{2}K	13	13	E′	32 998		
13	^{4}I	13	7	E′	6 760	6 745	15	81	^{2}K	13	3	E″	33 005		
14	^{4}I	13	9	E″	6 773	6 778	−5	82	^{2}K	13	5	E′	33 046		
15	^{4}I	13	11	E′	6 810	6 819	−9	83	^{2}P	1	1	E′	33 093		
16	^{4}I	11	11	E′	10 260			84	^{2}K	13	11	E′	33 187		
17	^{4}I	11	3	E″	10 276			85	^{2}K	13	9	E″	33 212		
18	^{4}I	11	1	E′	10 291			86	^{2}K	13	7	E′	33 212		
19	^{4}I	11	7	E′	10 321	10 318	3	87	^{4}G	5	3	E″	33 263		
20	^{4}I	11	5	E′	10 343	10 346	−3	88	^{4}G	5	5	E′	33 308		
21	^{4}I	11	9	E″	10 349			89	^{4}G	5	1	E′	33 429		
22	^{4}I	9	9	E″	12 350			90	^{4}G	7	5	E′	33 982	33 967	15
23	^{4}I	9	5	E′	12 422			91	^{4}G	7	1	E′	34 027	34 004	23
24	^{4}I	9	1	E′	12 528			92	^{4}G	7	3	E″	34 058	34 042	16
25	^{4}I	9	3	E″	12 612			93	^{4}G	7	7	E′	34 119	34 131	−12
26	^{4}I	9	7	E′	12 654			94	^{2}D	5	5	E′	34 852	34 866	−14
27	^{4}F	9	1	E′	15 319	15 328	−9	95	^{2}D	5	1	E′	34 898	34 883	15
28	^{4}F	9	9	E″	15 349	15 354	−5	96	^{2}D	5	3	E″	34 909	34 909	0
29	^{4}F	9	3	E″	15 399	15 392	7	97	^{2}H	9	7	E′	36 425		
30	^{4}F	9	7	E′	15 430	15 425	5	98	^{2}H	9	9	E″	36 457		
31	^{4}F	9	5	E′	15 445	15 442	3	99	^{2}H	9	1	E′	36 536		
32	^{4}S	3	3	E″	18 496	18 486	10	100	^{2}H	9	5	E′	36 630		
33	^{4}S	3	1	E′	18 509	18 501	8	101	^{2}H	9	3	E″	36 671		
34	^{2}H	11	7	E′	19 189	19 184	5	102	^{4}D	5	1	E′	38 555		
35	^{2}H	11	5	E′	19 224	19 215	9	103	^{4}D	5	5	E′	38 601		
36	^{2}H	11	9	E″	19 228	19 222	6	104	^{4}D	5	3	E″	38 611		
37	^{2}H	11	11	E′	19 275	19 277	−2	105	^{4}D	7	5	E′	39 234	39 217	17
38	^{2}H	11	3	E″	19 292	19 294	−2	106	^{4}D	7	3	E″	39 274	39 264	10
39	^{2}H	11	1	E′	19 332	19 340	−8	107	^{4}D	7	1	E′	39 281	39 300	−19
40	^{4}F	7	5	E′	20 557	20 567	−10	108	^{4}D	7	7	E′	39 362	39 352	10
41	^{4}F	7	3	E″	20 607	20 611	−4	109	^{2}I	11	5	E′	41 069		
42	^{4}F	7	7	E′	20 637	20 644	−7	110	^{2}I	11	9	E″	41 102		
43	^{4}F	7	1	E′	20 683	20 690	−7	111	^{2}I	11	1	E′	41 185		
44	^{4}F	5	3	E″	22 268	22 273	−5	112	^{2}I	11	11	E′	41 195		
45	^{4}F	5	5	E′	22 273	22 280	−7	113	^{2}I	11	3	E″	41 215		
46	^{4}F	5	1	E′	22 303	22 312	−9	114	^{2}I	11	5	E′	41 292		
47	^{4}F	3	3	E″	22 617	22 617	0	115	^{2}L	17	1	E′	41 601		
48	^{4}F	3	1	E′	22 631	22 636	−5	116	^{2}L	17	3	E″	41 620		
49	^{2}G	9	9	E″	24 527	24 550	−23	117	^{2}L	17	5	E′	41 652		
50	^{2}G	9	5	E′	24 586	24 579	7	118	^{2}L	17	13	E′	41 707		
51	^{2}G	9	1	E′	24 679	24 680	−1	119	^{2}L	17	15	E″	41 711		
52	^{2}G	9	3	E″	24 744	24 743	1	120	^{2}L	17	17	E′	41 718		
53	^{2}G	9	7	E′	24 778	24 782	−4	121	^{2}L	17	7	E′	41 738		
54	^{4}G	11	7	E′	26 403	26 406	−3	122	^{2}L	17	9	E″	41 752		
55	^{4}G	11	9	E″	26 427	26 423	4	123	^{2}L	17	11	E′	41 755		
56	^{4}G	11	5	E′	26 431	26 431	0	124	^{4}D	3	3	E″	42 279		
57	^{4}G	11	3	E″	26 531	26 533	−2	125	^{4}D	3	1	E′	42 288		
58	^{4}G	11	11	E′	26 551	26 551	0	126	^{2}D	3	1	E′	42 857		
59	^{4}G	11	1	E′	26 585	26 585	0	127	^{2}D	3	3	E″	42 864		
60	^{4}G	9	7	E′	27 426	27 438	−12	128	^{2}I	13	11	E′	43 506		
61	^{4}G	9	1	E′	27 457	27 446	11	129	^{2}I	13	9	E″	43 538		
62	^{4}G	9	3	E″	27 463	27 464	−1	130	^{2}I	13	7	E′	43 558		
63	^{4}G	9	5	E′	27 475	27 485	−10	131	^{2}I	13	1	E′	43 672		
64	^{4}G	9	9	E″	27 481	27 497	−16	132	^{2}I	13	3	E″	43 701		
65	^{2}K	15	1	E′	27 721			133	^{2}I	13	5	E′	43 725		
66	^{2}K	15	3	E″	27 753			134	^{2}I	13	13	E′	43 815		
67	^{2}K	15	15	E″	27 785			135	^{4}D	1	1	E′	47 050		
68	^{2}K	15	5	E′	27 820										

[a] Identifies the *principal* $SLJM_J$ components of the eigenvectors. [b] Irrep label in the D_3 double-group. [c] Calculated by using the Hamiltonian parameter values listed in Table III. [d] With $1/\lambda$(air) to $1/\lambda$(vacuum) correction. Uncertainties in the energy-level locations are ca. ±4 cm^{-1} (on average). [e] Difference between calculated and observed energies.

average value of $S(\pi)/[S(\sigma) + S(\pi)]$ is 0.85 (or 85% π-polarized character). The transition line strengths determined from unpolarized *axial* absorption intensity measurements (according to eq 4) closely match the $S(\sigma)$ data.

Deviations of the measured P values from 1 (for E″ → E″ transitions) or from -1 (for the E″ → E′ transitions) can be

Table III. Energy Parameters for the $4f^{11}$ Electronic Configuration of Er^{3+} in $Na_3[Er(ODA)_3]\cdot 2NaClO_4\cdot 6H_2O$

param[a]	value[b]/cm^{-1}	param[a]	value[b]/cm^{-1}
E_{av}	35742	M^2	$0.56M^0$
F^2	99823	M^4	$0.38M^0$
F^4	70707	P^2	798
F^6	49831	P^4	$0.75P^2$
α	18.9	P^6	$0.50P^2$
β	−660	B_{20}	−89
γ	1672	B_{40}	−881
T^2	510	B_{43}	−745
T^3	35	B_{60}	374
T^4	85	B_{63}	661
T^6	−344	B_{66}	648
T^7	315	N^c	65
T_8	512	σ^d	9.6
ζ_{so}	2378		
M^0	4.10		

[a] See eqs 1–3 in the text. [b] Determined by fitting the observed energy levels listed in Table II. [c] Number of assigned energy levels included in the parametric data fits. [d] Root-mean-square deviation between calculated and observed energies (in cm^{-1}).

Table IV. Major-Component Analysis of $4f^{11}[SL]J$ State Vectors

multiplet label[a]	energy[b]/cm^{-1} exptl	energy[b]/cm^{-1} calcd	major SL (term) components[c]
$^4I_{15/2}$	n.d.	215	^4I (97%) + ^2K (3%)
$^4I_{13/2}$	6700	6703	^4I (99%) + ^2K (1%)
$^4I_{11/2}$	n.d.	10307	^4I (82%) + $^2H(2)$ (15%)
$^4I_{9/2}$	n.d.	12513	^4I (52%) + $^2H(2)$ (18%) + ^4F(13%)
$^4F_{9/2}$	15388	15388	^4F (59%) + ^4I (27%) + $^2G(1)$ (8‰)
$^4S_{3/2}$	18494	18502	^4S (68%) + ^2P (19%) + $^2D(1)$ (8%)
$^2H_{11/2}$	19255	19256	$^2H(2)$ (46%) + ^4G (37%) + ^4I (15%)
$^4F_{7/2}$	20628	20621	^4F (92%) + $^2G(1)$ (4%) + $^2G(2)$ (3%)
$^4F_{5/2}$	22288	22282	^4F (84%) + $^2D(1)$ (13%)
$^4F_{3/2}$	22626	22624	^4F (62%) + $^2D(1)$ (21%) + ^4S (16%)
$^2G_{9/2}$	24667	24663	^4F (24%) + $^2G(1)$ (19%) + $^2G(2)$ (16%) + $^2H(2)$ (16%) + ^4I (12%) + $^2H(1)$ (7%) + ^4G (6%)
$^4G_{11/2}$	26488	26488	^4G (59%) + $^2H(2)$ (27%) + $^2H(1)$ (10%)
$^4G_{9/2}$	27466	27461	^4G (80%) + $^2H(2)$ (14%) + ^4I (5%)
$^2K_{15/2}$	n.d.	27862	^2K (91%) + ^2L (6%) + ^4I (3%)
$^2G_{7/2}$	n.d.	28098	^4G (42%) + $^2G(1)$ (25%) + $^2G(2)$ (23%)
$^2P_{3/2}$	31604	31599	^2P (36%) + ^4F (24%) + $^2D(1)$ (20%) + ^4S (12%)
$^2K_{13/2}$	n.d.	33090	^2K (90%) + ^2I (9%) + ^4I (1%)
$^2P_{1/2}$	n.d.	33093	^2P (92%) + ^4D (8%)
$^4G_{5/2}$	n.d.	33333	^4G (91%) + $^2F(2)$ (4%) + $^2F(1)$ (3%)
$^4G_{7/2}$	34036	34046	^4G (53%) + $^2G(1)$ (28%) + $^2G(2)$ (16%)
$^2D_{5/2}$	34886	34886	$^2D(1)$ (56%) + $^2D(2)$ (16%) + ^4D(15%) + ^4F (14%)
$^2H_{9/2}$	n.d.	36544	$^2H(2)$ (33%) + $^2G(1)$ (23%) + $^2G(2)$ (16%) + ^4G (12%) + $^2H(1)$ (8%)
$^4D_{5/2}$	n.d.	38589	^4D (42%) + $^2D(1)$ (29%) + $^2D(2)$ (24%)
$^4D_{7/2}$	39283	39287	^4D (94%) + $^2F(1)$ (3%)

[a] These labels reflect the *principal SLJ* components of each multiplet. [b] Experimentally observed and calculated baricenters of the multiplet manifolds (determined from the energy level data shown in Table II). [c] The percent contributions are from calculations based on the Hamiltonian parameters listed in Table III.

attributed, in part, to the usual measurement imperfections inherent to polarized, single-crystal absorption studies. However, the degree of polarization "scrambling" observed in the ErODA spectra is larger than that observed in the spectra of other LnODA systems studied under similar measurement conditions. This suggests that in ErODA the trigonal symmetry axes of the $Er(ODA)_3^{3-}$ complexes are tilted away from the crystallographic c axis, but the tilts of these local axes are such as to preserve macroscopic cylindrical symmetry about the crystallographic c axis. In this structural model, the μ_z transition vector of a E″ → E″ transition would have projections on both the crystal c axis (μ_q, $q = 0$) *and* on a plane perpendicular to this axis (μ_q, $q = \pm 1$). Likewise, the μ_x and μ_y transition vectors of a E″ → E′ transition would have projections on both the $q = 0$ axis *and* on a plane perpendicular to this axis. For both types of transitions, the μ_q ($q = 0$) component of the electric dipole transition moment will contribute to π-polarized absorption intensity, and the μ_q ($q = \pm 1$) components will contribute to σ-polarized absorption intensity. If we define τ as the angle at which the $C_3(z)$ symmetry axis of a $Er(ODA)_3^{3-}$ complex is tilted away from the crystal c axis, then the P parameters of Table VIII may be related to τ according to

$$P = \frac{S(\pi) - S(\sigma)}{S(\pi) + S(\sigma)} = \pm(\cos^2\tau - \sin^2\tau) \qquad (14)$$

where the positive sign applies to E″ → E″ transitions and the negative sign applies to E″ → E′ transitions. For the E″ → E″ transitions listed in Table VIII, the average value of P is 0.70, which corresponds to $\tau \approx 22.5°$ in eq 14. For the E″ → E′ transitions, the average value of P is −0.54, which corresponds to $\tau \approx 28.5°$.

An alternative explanation for the observation of *mixed* ($\sigma + \pi$) polarization in the low-temperature orthoaxial absorption spectra may also be offered. In several previous studies it has been suggested that $Na_3[Ln(ODA)_3]\cdot 2NaClO_4\cdot 6H_2O$ systems undergo a low-temperature structural phase transition in which the crystal space group changes from $R32$ to $P321$, and the lanthanide site symmetry is reduced from D_3 to C_2 (attributable to movement of the Na^+ ions off 3-fold axes).[11,14,35,46] If this type of structural change occurs in ErODA, *and* if the "effective" ligand-field potential at the Er^{3+} ions reflects C_2 rather than D_3 symmetry, then our E′ and E″ state labels (and the selection rules of Table I) are no longer rigorously valid. In C_2 symmetry, the eigenstates of the system may contain admixtures of the erstwhile E′ and E″ states, and optical transitions between levels will exhibit polarization properties that reflect this admixture. This might explain our mixed-polarization line-intensity results. However, as was noted earlier, the crystal-field energy-level structure of

Table V. Comparison of Atomic Hamiltonian Parameters Reported for Er^{3+} in Crystalline Hosts

param[a]	values[b]/cm^{-1} ErODA[c]	$ErCl_3\cdot 6H_2O$[d]	Er^{3+}:$LaCl_3$[e]	Er^{3+}:LaF_3[f]	Er^{3+}:$LiYF_4$[g]
F^2	99823	99891	98220	97483	99230
F^4	70707	70646	70079	67904	70683
F^6	49831	49734	49625	54010	48375
ζ_{so}	2378	2380	2364	2376	2360
α	18.9	18.9	16.1	17.8	20.0
β	−660	−620	−607	−582	−589
γ	1672	1648	1787	[1800]	[1800]
T^2	510	518	286	[400]	[400]
T^3	35	34	48	43	[43]
T^4	85	76	14	73	[73]
T^6	−344	−340	−324	−271	[−271]
T^7	315	317	172	308	[308]
T^8	512	393	323	299	[299]
M^0	4.10	[4.5]	3.56	3.86	4.96
P^2	798	740	381	594	580

[a] See eq (2) in the text. [b] Values shown in square brackets were held fixed in performing calculated-to-empirical energy-level fits. [c] From Table III of present paper. [d] From ref 55. [e] From ref 56. [f] From ref 54. [g] From ref 57.

Table VI. Comparison of Crystal-Field Parameters Reported for Er^{3+} in Crystal Systems Having *Trigonal* (Er^{3+}) Site Symmetries

param	values/cm^{-1} ErODA (D_3)[a]	ErES (C_{3h})[b]	Er^{3+}:$LaCl_3$ (C_{3h})[c]
B_{20}	−89	−301	−272
B_{40}	−881	−731	−358
B_{43}	−745		
B_{60}	374	631	513
B_{63}	661		
B_{66}	648	−532	−306

[a] Present work. [b] From ref 58. ErES ≡ $Er(C_2H_5SO_4)_3\cdot 9H_2O$. [c] From ref 56.

Table VII. Comparison of Crystal-Field Energy Parameters Obtained for $Na_3[Ln(ODA)_3]\cdot 2NaClO_4\cdot 6H_2O$ Systems

param	values/cm^{-1}					
	NdODA[a]	SmODA[b]	EuODA[c]	GdODA[d]	HoODA[e]	ErODA[f]
B_{20}	56	−19	−91	−87	−88	−89
B_{40}	−1111	−941	−947	−952	−836	−881
B_{43}	−943	−837	−781	−845	−578	−745
B_{60}	577	606	411	803	531	374
B_{63}	1358	1112	1035	1197	777	661
B_{66}	886	794	755	961	672	648
N	116	144	61	60	105	65
σ	14.4	12.3	9.9	6.3	9.1	9.6

[a] From ref 39. [b] From ref 28. [c] From ref 33 and J. Quagliano (University of Virginia), unpublished results. [d] From ref 45. [e] From ref 43. [f] From Table III of present paper.

Table VIII. Polarized Line Strengths of Absorptive Transitions Originating from the Ground Crystal-Field Level of Er^{3+} in $Na_3[Er(ODA)_3]\cdot 2NaClO_4\cdot 6H_2O$

excited level[a]				line strengths[c]/10^{-42} esu^2 cm^2		
no.	multiplet	Γ	$\bar{\nu}$(air)[b]/cm^{-1}	$S(\sigma)$	$S(\pi)$	P[d]
27	$^4F_{9/2}$	E′	15332	6.6	1.1	−0.71
28		E″	15358	3.3	51.5	0.88
29		E″	15396	1.9	32.2	0.89
30		E′	15429	47.2	8.4	−0.70
31		E′	15446	38.7	5.8	−0.74
32	$^4S_{3/2}$	E″	18491	2.9	8.3	0.48
33		E′	18506	14.0	7.4	−0.31
34	$^2H_{11/2}$	E′	19189	10.0	4.5	−0.38
35		E′	19220	27.9	10.7	−0.45
36		E″	19227	11.1	36.7	0.54
37		E′	19282	25.9	6.8	−0.58
38		E″	19299	3.0	31.1	0.82
39		E′	19345	11.8	2.7	−0.63
40	$^4F_{7/2}$	E′	20573	13.6	3.7	−0.57
41		E″	20617	2.5	14.3	0.70
42		E′	20650	14.4	4.7	−0.51
43		E′	20696	4.6	0.9	−0.67
44	$^4F_{5/2}$	E″	22279	5.6	34.8	0.72
45		E′	22286	20.1	7.4	−0.46
46		E′	22318	13.6	3.3	−0.61
47	$^4F_{3/2}$	E″	22623	7.8	18.8	0.41
48		E′	22642	20.3	9.1	−0.38
49	$^2G_{9/2}$	E″	24557	2.3	12.6	0.69
50		E′	24586	7.5	3.6	−0.35
51		E′	24687	33.2	6.6	−0.67
52		E″	24750	2.2	11.6	0.68
53		E′	24789	22.3	4.6	−0.66
54	$^4G_{11/2}$	E′	26413	29.0	14.2	−0.34
55		E″	26430	6.4	68.7	0.83
56		E′	26438	38.1	n.d.	n.d.
57		E″	26540	7.4	43.5	0.71
58		E′	26558	50.6	13.1	−0.59
59		E′	26592	9.3	7.9	−0.08

[a] Numbering scheme, multiplet labels, and crystal-field symmetry labels (Γ) correspond to those used in Table II. [b] Transition frequency expressed in wavenumbers, $1/\lambda$(air). [c] Line strengths were determined from 20 K absorbance data according to eq 5 (see text), and they are expressed in units of 10^{-42} esu^2 cm^2 (1 esu cm = 3.3356×10^{-30} C m). n.d. = not determined. Uncertainties in the line-strength values are ca. $\pm 0.2 \times 10^{-42}$ esu^2 cm^2 (on average). [d] $P = (S(\pi) - S(\sigma))/(S(\pi) + S(\sigma))$.

$Er^{3+}(4f^{11})$ in ErODA appears to be satisfactorily accounted for by a model Hamiltonian of D_3 symmetry.

Spectra. A survey *axial* absorption spectrum over the 6500–27000-cm^{-1} wavenumber range is shown in Figure 1. This spectrum spans the 11 lowest energy multiplet-to-multiplet transition manifolds that originate from the $^4I_{15/2}$ (ground) multiplet. Note, however, that the $^4I_{15/2} \rightarrow {}^4I_{9/2}$ transition (centered near 12500 cm^{-1}) is too weak to appear in this spectrum.

Comparisons of σ- versus π-polarized *orthoaxial* absorption spectra are shown in Figures 2 and 3 for the $^4I_{15/2} \rightarrow {}^4F_{9/2}$ and $^4I_{15/2} \rightarrow {}^2H_{11/2}$ transition regions, respectively. Spectral features assigned to transitions from the lowest (ground) crystal-field level

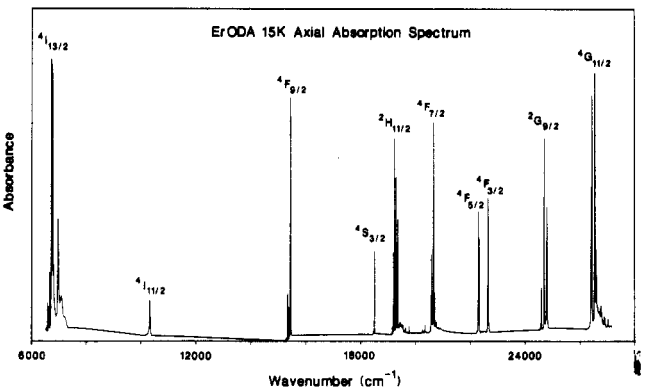

Figure 1. Survey *axial* absorption spectrum recorded between 6500 and 27000 cm^{-1} at a sample temperature of 15 K.

Table IX. Absorption Dissymmetry Factors Determined from Axial Circular Dichroism and Absorption Measurements

CD/abs line no.[a]	$\bar{\nu}$(air)/cm^{-1}	excited level[b]		$10^2 g_{cd}$[c]
27	15332	$^4F_{9/2}$	E′	+1.1
28	15358		E″	+1.2
29	15396		E″	+6.0
30	15429		E′	−0.3
31	15446		E′	−0.3
34	19189	$^2H_{11/2}$	E′	−0.4
35	19220		E′	−(very small)
36	19227		E″	+(large)
37	19282		E′	−(very small)
38	19299		E″	+4.8
39	19345		E′	−0.2
40	20573	$^4F_{7/2}$	E′	−0.2
41	20617		E″	+2.6
42	20650		E′	−0.2
43	20696		E′	−0.3
44	22279	$^4F_{5/2}$	E″	+(large)
45	22286		E′	(very small)
46	22318		E′	−0.3
47	22623	$^4F_{3/2}$	E″	+1.1
48	22642		E′	−0.2
49	24557	$^2G_{9/2}$	E″	+11.2
50	24586		E′	−0.5
51	24687		E′	−0.2
52	24750		E″	+2.2
53	24789		E′	−0.4

[a] As shown in Figures 4–8. [b] All transitions originate from the E″ *ground* crystal-field level of the $^4I_{15/2}$ multiplet manifold. [c] Absorption dissymmetry factor defined according to eq 12. Uncertainties in the g_{cd} values are $\pm 0.1 \times 10^{-2}$ (or less).

of $^4I_{15/2}$ are identified by numbers that label the excited level of the transition (see Table II for the numbering scheme and level assignments). Unnumbered features correspond to "hot" transitions that originate from the second lowest energy crystal-field level of $^4I_{15/2}$ (level no. 2 in Table II). The spectra shown in Figures 2 and 3 illustrate the degree of σ- and π-polarization mixing in the E″ → E″ and E″ → E′ crystal-field transitions.

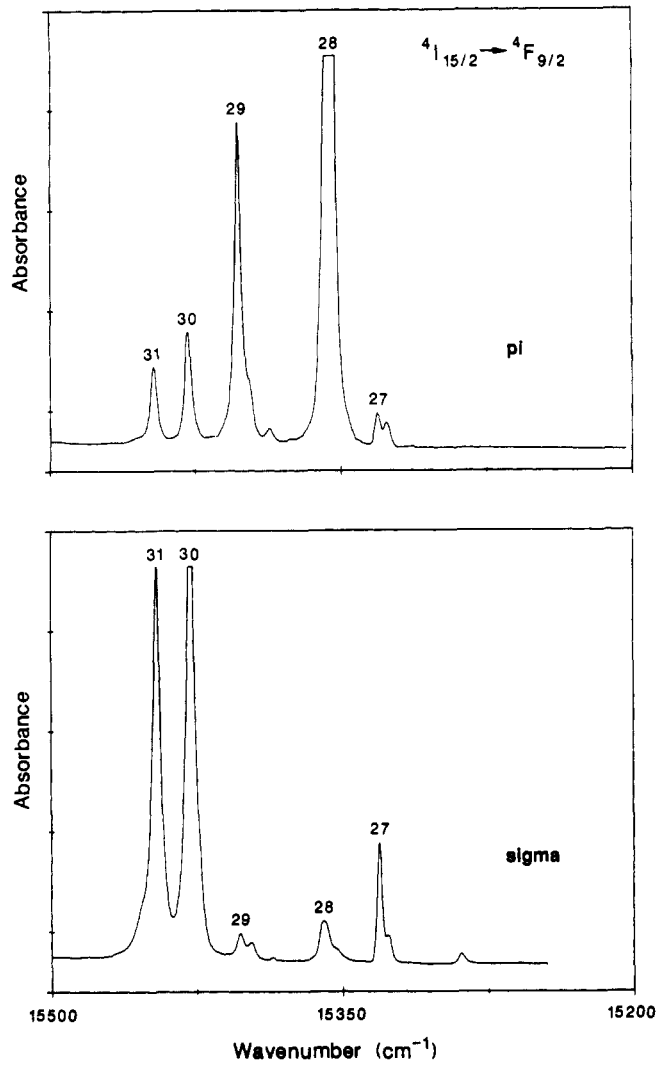

Figure 2. σ- and π-polarized *orthoaxial* absorption spectra recorded in the $^4I_{15/2} \rightarrow {}^4F_{9/2}$ transition region at a sample temperature of ~20 K.

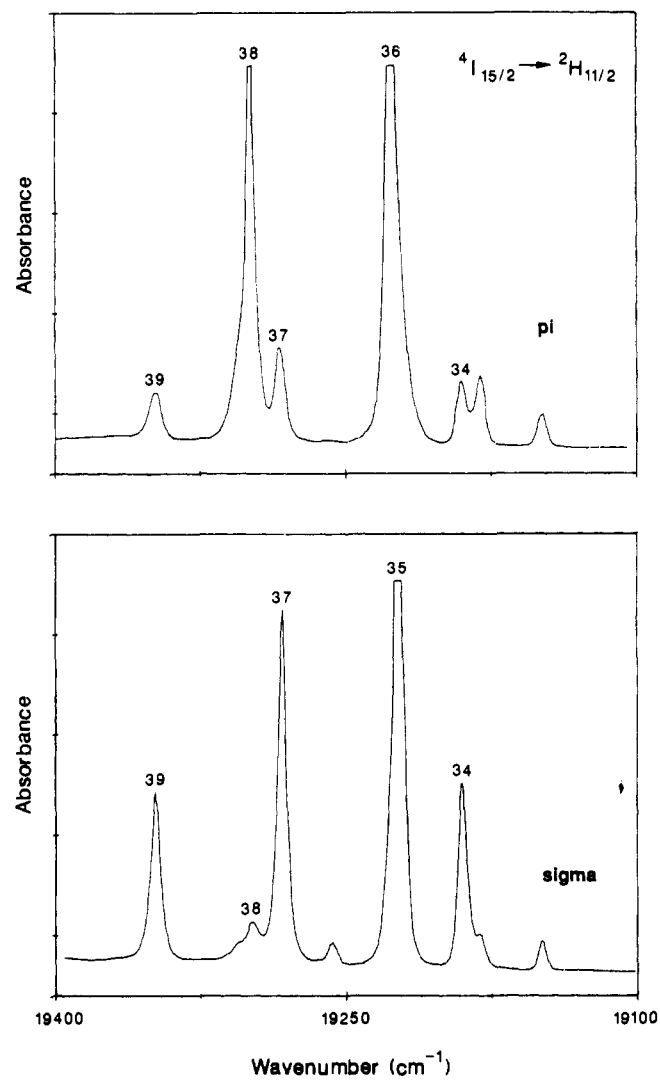

Figure 3. σ- and π-polarized *orthoaxial* absorption spectra recorded in the $^4I_{15/2} \rightarrow {}^2H_{11/2}$ transition region at a sample temperature of ~20 K.

Identical absorbance scales are used in the σ and π spectra plotted in Figures 2 and 3.

Axial absorption and circular dichroism (CD) spectra are shown in Figures 4–8 for the $^4I_{15/2} \rightarrow {}^4F_{9/2}$, $^2H_{11/2}$, $^4F_{7/2}$, $^4F_{5/2}$, $^4F_{3/2}$, and $^2G_{9/2}$ transition regions, respectively. Spectral features assigned to transitions from the ground crystal-field level of $^4I_{15/2}$ are numbered according to the same scheme described above for Figures 2 and 3, and all unnumbered features are assignable to hot transitions that originate from level no. 2 of $^4I_{15/2}$ (see Table II). All of the spectra shown in Figures 4–8 were obtained on a crystal of thickness 0.08 cm, at a temperature of ~20 K. The CD intensity scales are given in millidegree (mdeg) units of *ellipticity*. One mdeg of ellipticity corresponds to a differential absorbance of $\Delta A = A_L - A_R = 3.032 \times 10^{-5}$, where A_L and A_R denote decadic absorbances for left- and right-circularly polarized light, respectively.

Among the spectral features numbered in Figures 2–8, the following are assigned to E″ → E′ crystal-field transitions: 27, 30, and 31 (Figures 2 and 4); 34, 35, 37, and 39 (Figures 3 and 5); 40, 42, and 43 (Figure 6); 45, 46, and 48 (Figure 7); 50, 51, and 53 (Figure 8). The following are assigned to E″ → E″ transitions: 28 and 29 (Figures 2 and 4); 36 and 38 (Figures 3 and 5); 41 (Figure 6); 44 and 47 (Figure 7); 49 and 52 (Figure 8). Absorption dissymmetry factors determined for these transitions are listed in Table IX. The dissymmetry factors are ratios of CD to absorption intensity ($\Delta A/A$) within specified transition regions, and they are related to transition rotatory strengths and absorption line strengths according to eq 12. Note from Table IX that the largest dissymmetry factors are observed in E″ → E″ transitions.

Discussion

The energy-level structure observed for the $4f^{11}$ electronic configuration of Er^{3+} in trigonal $Na_3[Er(ODA)_3]\cdot 2NaClO_4\cdot 6H_2O$ can be reasonably well accounted for by a model Hamiltonian that assumes D_3 crystal-field symmetry. Calculations based on a parametrized form of this Hamiltonian yield energy levels that closely match those located and assigned from experiment. Among the 108 crystal-field levels associated with the 24 lowest energy $4f^{11}$ J-multiplets of Er^{3+} (in D_3 symmetry), 65 were located and assigned from experiment, and the root-mean-square deviation between the calculated and observed locations of these levels is 9.6 cm^{-1}. The root-mean-square deviation between calculated and observed J-multiplet baricenter energies is 5 cm^{-1} (see Table IV). The parameters in our *atomic* Hamiltonian ($\hat{H}_a$, defined by eq 2) have values that are remarkably similar to those reported for Er^{3+} in $ErCl_3\cdot 6H_2O$ (see Table V). In the latter system, each erbium ion is coordinated to six water oxygen atoms and two chloride ions located at the corners of a square antiprism of approximate D_{4d} symmetry.[54]

The crystal-field parameters derived from our analysis of ErODA energy levels are qualitatively similar to those determined previously for other LnODA systems (see Table VII). The HoODA parameters show the closest match with the ErODA parameters, as might be expected since Ho^{3+} ($4f^{10}$) and Er^{3+} ($4f^{11}$) occupy adjacent positions in the lanthanide series.

In previous studies of electronic energy-level structure and optical properties of NdODA,[39,40] SmODA,[28-30] EuODA,[33,34] and HoODA,[43,44] we performed detailed parametric analyses of transition line-strength data and derived intensity parameters that

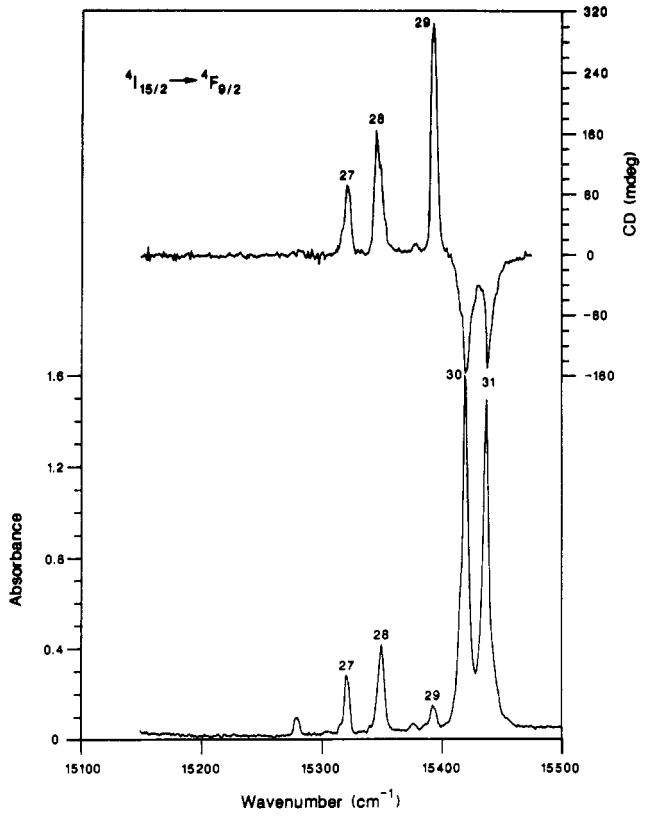

Figure 4. *Axial* CD (top trace) and absorption (bottom trace) spectra recorded in the $^4I_{15/2} \rightarrow {}^4F_{9/2}$ transition region at a sample temperature of ~20 K.

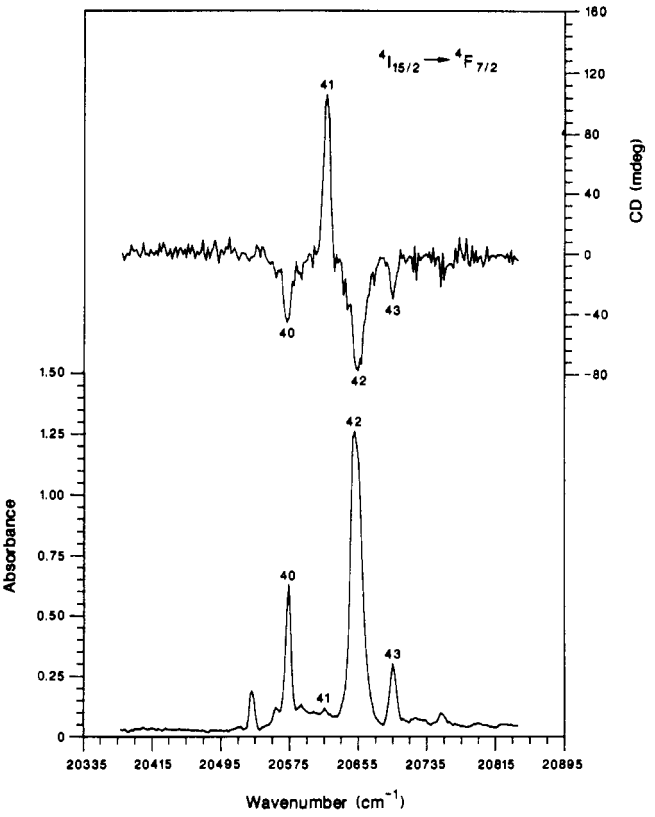

Figure 6. *Axial* CD (top trace) and absorption (bottom trace) spectra recorded in the $^4I_{15/2} \rightarrow {}^4F_{7/2}$ transition region at a sample temperature of ~20 K.

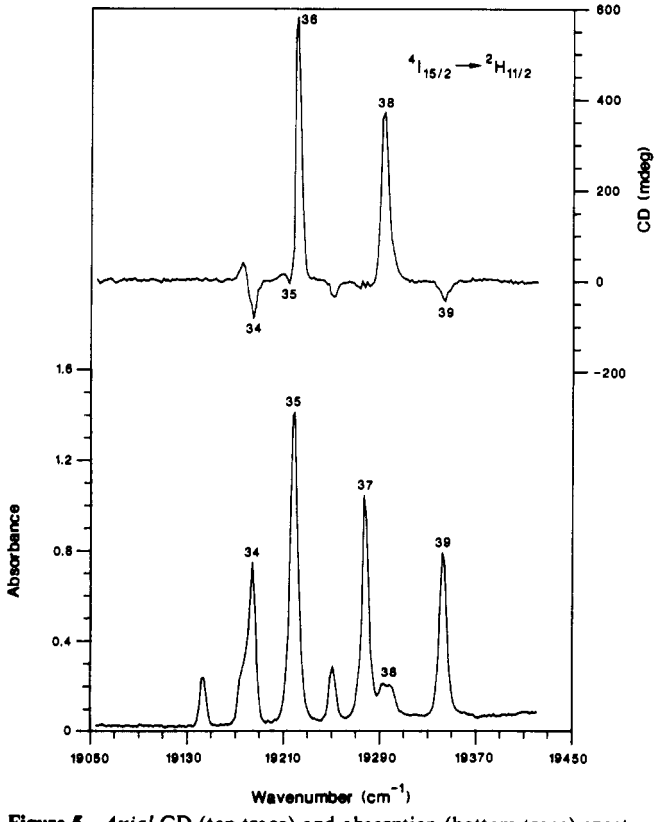

Figure 5. *Axial* CD (top trace) and absorption (bottom trace) spectra recorded in the $^4I_{15/2} \rightarrow {}^2H_{11/2}$ transition region at a sample temperature of ~20 K.

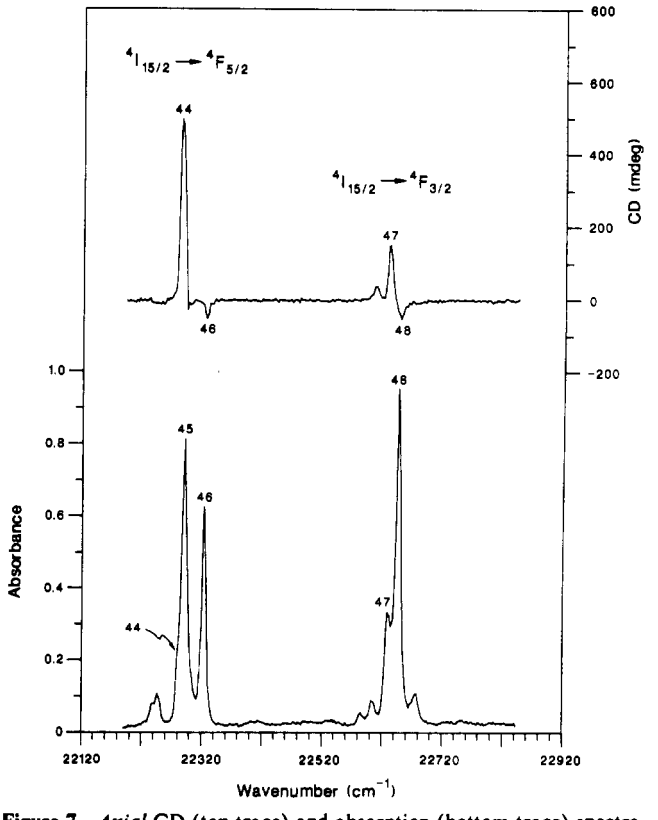

Figure 7. *Axial* CD (top trace) and absorption (bottom trace) spectra recorded in the $^4I_{15/2} \rightarrow {}^4F_{5/2}$, $^4F_{3/2}$ transition region at a sample temperature of ~20 K.

could be related to 4f–4f electric dipole transition mechanisms and to odd-parity lanthanide–ligand-field interactions. In those analyses, it was assumed that the lanthanide site symmetry is D_3 and the trigonal symmetry axis at each lanthanide site is aligned parallel to the crystallographic c axis in $Na_3[Ln(ODA)_3]\cdot 2NaClO_4\cdot 6H_2O$. The results obtained from those analyses provided the basis for calculations of "simulated" spectra over transition regions that were difficult to characterize empirically,

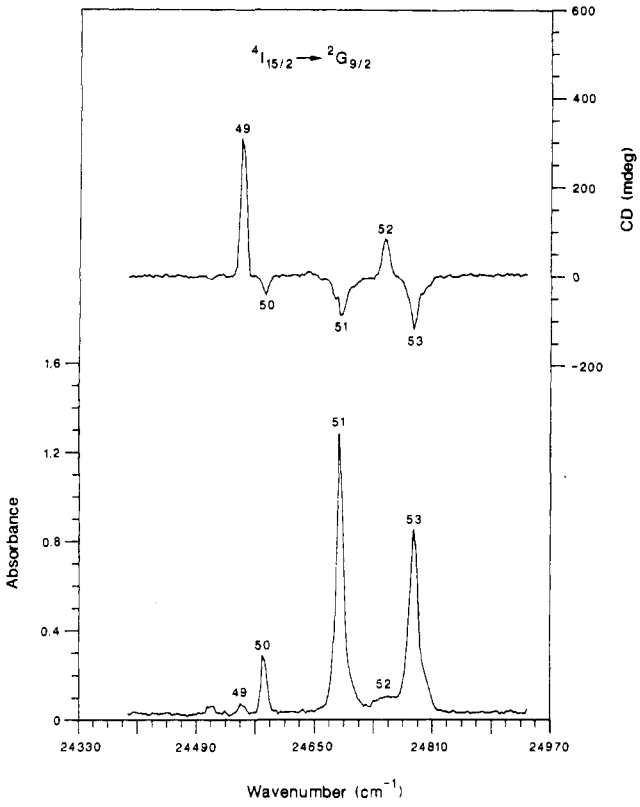

Figure 8. *Axial* CD (top trace) and absorption (bottom trace) spectra recorded in the $^4I_{15/2} \rightarrow {}^2G_{9/2}$ transition region at a sample temperature of ~20 K.

and they also provided useful diagnostic checks on the quality of the eigenvectors generated by our model Hamiltonian. Detailed analyses of the ErODA intensity data are not reported here because the quantitative line-strength data and the CD results suggest structural distortions and/or electronic perturbations (at the Er^{3+} sites) that cannot be incorporated unambiguously into our intensity model.

Spectroscopic evidence indicates that *all* of the $Na_3[Ln(ODA)_3]\cdot 2NaClO_4\cdot 6H_2O$ systems undergo at least some structural change between room temperature and 5 K, but the optical consequences of this change appear to be greater for ErODA than for the other LnODA systems. The structural change does not destroy the macroscopic uniaxial symmetry of the crystals, but it does cause a partial breakdown of optical polarization selection rules based on the presumption of $R32$ space-group symmetry and D_3 lanthanide-site symmetry (i.e., the room-temperature structure). It has been proposed that the low-temperature structural changes reduce the space-group symmetry to $P321$ and the lanthanide-site symmetry to C_2, and they have been attributed to movement of the Na^+ ions off 3-fold axes *and/or* a tilting of $Ln(ODA)_3^{3-}$ trigonal axes away from the crystallographic 3-fold symmetry axis.[11,14,35,46] The low-temperature absorption and CD results obtained for ErODA are compatible with these proposals, but they are not adequate for carrying out detailed diagnostic analyses of low-temperature structure.

Earlier in this paper, we correlated the polarization parameter P to the average angle-of-tilt (τ) between the C_3 symmetry axis of a $Er(ODA)_3^{3-}$ complex and the crystallographic c axis (see eq 14). Using averages of the P data shown in Table VIII (for E″ → E″ and E″ → E′ transitions), we calculated tilt angles of between 22 and 28°. These results are interesting and possibly informative, but they must be considered with some circumspection. They are based on a model in which it is assumed that the crystal-field states of Er^{3+} ($4f^{11}$) reflect the *local* trigonal symmetry of the $Er(ODA)_3^{3-}$ complexes and are not perturbed by structural entities located outside of these complexes. This assumption would appear to be supported by the success of our energy-level analysis, which is based entirely on the use of a D_3 crystal-field Hamiltonian. However, it is possible that the 4f–4f transition intensities (and polarizations) are much more sensitive to *nonlocal* perturbations that reflect a symmetry lower than D_3 (e.g., C_2). If this is the case, then the true spectroscopic states must be considered as having only *approximate* D_3 symmetry (E′ or E″), the selection rules of Table I are nonrigorous, and deviations of the observed P values from ±1 may be attributed, at least in part, to crystal-field perturbations of symmetry lower than D_3 (*or* C_3).

Acknowledgment. This work was supported by the U.S. National Science Foundation (NSF Grant CHE-8820180 to F.S.R.). We also gratefully acknowledge help and advice from Dr. Michael F. Reid and Dr. David H. Metcalf.